INTERNATIONAL JOURNAL OF ROBUST AND NONLINEAR CONTROL
Int. J. Robust. Nonlinear Control 2016; **00**:1–16
Published online in Wiley InterScience (www.interscience.wiley.com). DOI: 10.1002/rnc

A method to construct reduced-order parameter varying models

Jennifer Annoni*and Peter Seiler

Aerospace Engineering and Mechanics, University of Minnesota

SUMMARY

This paper describes a method to construct reduced-order models for high-dimensional nonlinear systems. It is assumed that the nonlinear system has a collection of equilibrium operating points parameterized by a scheduling variable. First, a reduced-order linear system is constructed at each equilibrium point using state, input, and output data. This step combines techniques from proper orthogonal decomposition, dynamic mode decomposition, and direct subspace identification. This yields discrete-time models that are linear from input to output but whose state matrices are functions of the scheduling parameter. Second, a parameter varying linearization is used to connect these linear models across the various operating points. The key technical issue in this second step is to ensure the reduced-order linear parameter varying system approximates the nonlinear system even when the operating point changes in time. Copyright © 2016 John Wiley & Sons, Ltd.

Received . . .

KEY WORDS: dynamic mode decomposition; reduced-order modeling; parameter varying

1. INTRODUCTION

This paper describes a method to construct a reduced-order model for high-dimensional nonlinear systems. The work is motivated by the control of systems that involve fluid and/or structural dynamics. One specific example is wind farm control. The overall performance of a wind farm can be improved through proper coordination of the turbines [1]. High-fidelity computational fluid dynamic models have been developed for wind farms [2, 3]. These high-fidelity models are accurate but are not suitable for controller design due to their computational complexity. A second example involves the control of flexible aircraft. More fuel efficient aircraft can be designed by reducing structural weight thus leading to increased flexibility [4]. The vibrational modes can significantly degrade the performance and can even lead to aeroelastic instabilities (flutter) [4, 5]. High-fidelity, computational fluid/structural models also exist for this application [6, 7] but these are also too complex for control design. Simplified, control-oriented models are needed in both of these examples.

A variety of reduced-order modeling techniques have been developed by the fluid dynamics and controls communities. These methods range from analytical reduced-order modeling, such as balanced truncation [8], to data-driven reduced-order modeling such as system identification [9] where a low-dimensional system is identified to describe the dynamics of a high-dimensional system. Subspace techniques have been applied to balanced truncation to perform model reduction on nonlinear systems [10]. One main drawback to system identification is that the states of the identified model do not have physical meaning. When addressing parameter varying systems, there is a state consistency issue that stems from the lack of physical meaning in the states. For example,

*Correspondence to: University of Minnesota 110 Union St SE, Minneapolis, MN 55455 . E-mail: anno0010@umn.edu

eigensystem realization algorithm (ERA) is a popular method in the system identification literature that uses impulse response data to construct a linear model of the system [11]. This method has been extended to generic input signals and time varying systems [12–15]. In the fluid dynamics literature, proper orthogonal decomposition (POD) is a standard method where the state is projected onto a low-dimensional subspace of POD modes constructed using data from the high-order system [16–18]. POD modes have been used to construct reduced-order models that can be used for control such as balanced POD [19, 20]. However, balanced POD requires the simulation of the adjoint of the system and this is not available for experiments. ERA has connections to BPOD [11, 21] where the adjoint does not need to be simulated under certain circumstances. Lastly, dynamic mode decomposition (DMD) is a more recent approach that fits time-domain data with linear dynamics on a reduced-order subspace [22–24]. DMD computes the spatial modes of a system at a single frequency and has ties to the Koopman operator [25–27]. DMD was developed for autonomous systems and was extended to include control inputs, i.e. DMD with control (DMDc) in [28].

This paper describes an extension of DMDc to construct reduced-order linear parameter varying (LPV) models that approximate high-order nonlinear models. The nonlinear system is assumed to have a parameterized collection of equilibrium operating points. For example, the free-stream wind speed and wind direction parameterizes the equilibrium condition in a wind farm. Related work on this particular topic has been done looking at flexible aircraft [29–31]. Many studies use linear methods such as Krylov methods [32, 33]. The proposed approach in this paper involves two steps. First, POD and direct subspace identification are combined to construct an input-output reduced-order model (IOROM). This terminology has been used in [29]. This step is similar to DMDc [28], which can be used to construct a reduced-order linear model at one operating condition. Specifically, this step uses direct N4SID subspace identification [9] on a low dimensional subspace spanned by POD modes. Second, the reduced-order models constructed at fixed operating conditions are "stitched" together using a parameter varying linearization (Section 2.3). The key technical issue is that the states of the reduced-order model must have a consistent meaning across all operating conditions (as described in Section 2.3.2). This state consistency issue has been addressed in other studies [34]. The difference in this paper is that the parameter is allowed to vary in time for a given simulation. The approach used in the paper handles this issue by constructing a single reduced-order subspace that is used at all operating conditions. This approach and the LPV linearization method is demonstrated on a nonlinear actuator disk example often used in wind farm control literature with more than 20,000 states (Section 3). Lastly, Section 4 will address conclusions and future work.

2. REDUCED-ORDER MODELING APPROACH FOR PARAMETER VARYING SYSTEMS

This section describes, in detail, the proposed method that accomplishes the criteria specified above. The proposed method combines approaches in the fluid dynamics and controls communities.

2.1. Criteria

There are a variety of methods in the controls and fluid dynamics literature that attempt to construct low-order models to describe the dominant dynamics of a high-dimensional system. The goal of this paper is to develop a method that can achieve the following:

- *Handles* $> 10^5$ *states*: The approach can be used develop low-order representations of fluid dynamic problems. Typical fluid dynamic problems can have more than a million states.
- *Handle inputs and outputs*: The objective is to develop low-order models for control design on systems with controllable inputs and measurable outputs, e.g. wind farms and flexible aircraft.
- *Adjoint-free*: Some existing methods require the use of a model adjoint. Our goal is to avoid the use of such adjoints so that the proposed method can be applied to either experimental data or to simulation models.
- *Reduced-order states have physical meaning*: The state of the reduced-order system can be used to approximately reconstruct the full-order state and can assist in the state consistency issue faced by parameter varying systems.

- *Can be used for parameter varying systems*: This is important for nonlinear systems where the dynamics change significantly over the entire operating range, e.g. wind farms and flexible aircraft.

2.2. Input-Output Reduced-Order Modeling

The approach will be summarized in this subsection for time-invariant (LTI) systems at a single operating point, but will be extended to include LPV models in Section 2.3. This paper addresses the use of this technique to develop an input-output reduced-order model (IOROM) that does not require adjoints and where the states have some physical meaning. In this section, an extension of DMDc [28] is presented as a combination of POD and system identification. It should be noted that DMD modes can be constructed from the reduced-order model. This paper will focus on the construction of the reduced-order model rather than the evaluation of the DMD modes.

Consider a discrete-time nonlinear system:

$$x_{k+1} = f(x_k, u_k) \tag{1}$$
$$y_k = h(x_k, u_k) \tag{2}$$

where $x \in \mathbb{R}^{n_x}$, $u \in \mathbb{R}^{n_u}$, and $y \in \mathbb{R}^{n_y}$ are the state, input, and output vectors.

A collection of snapshot measurements are obtained via simulation or experiments by exciting the system. Snapshots are taken from the nonlinear system and the states, inputs, and outputs are recorded as:

$$X_0 = \begin{bmatrix} x_0 & x_1 & \dots & x_{m-1} \end{bmatrix} \in \mathbb{R}^{n_x \times n_s} \tag{3}$$
$$X_1 = \begin{bmatrix} x_1 & x_2 & \dots & x_m \end{bmatrix} \in \mathbb{R}^{n_x \times n_s} \tag{4}$$
$$U_0 = \begin{bmatrix} u_0 & u_1 & \dots & u_{m-1} \end{bmatrix} \in \mathbb{R}^{n_u \times n_s} \tag{5}$$
$$Y_0 = \begin{bmatrix} y_0 & y_1 & \dots & y_{m-1} \end{bmatrix} \in \mathbb{R}^{n_y \times n_s} \tag{6}$$

where n_s is the number of snapshots.

The proposed variation of DMDc attempts to fit the snapshot measurements to a linear discrete-time system:

$$x_{k+1} = Ax_k + Bu_k \tag{7}$$
$$y_k = Cx_k + Du_k \tag{8}$$

The state matrices (A, B, C, D) have the dimensions compatible to those of (x, u, y). The matrices (A, B, C, D) can be constructed to fit the snapshot data with minimal least-squares cost as in direct N4SID [9]. However, this becomes intractable for large systems. Typical fluid dynamic systems have on the order of millions of states. The proposed solution is to project the state onto a low-dimensional subspace to make the least squares computation tractable. Let $Q \in \mathbb{R}^{n_x \times r}$ with $r < n$ have columns that form an orthonormal basis for a projection subspace. The IOROM is expressed in terms of the projected state $z := Q^T x \in \mathbb{R}^r$ is given by:

$$z_{k+1} = (Q^T AQ)z_k + (Q^T B)u_k := Fz_k + Gu_k \tag{9}$$
$$y_k = (CQ)z_k + Du_k := Hz_k + Du_k \tag{10}$$

The matrices in the reduced-order system have dimensions $F \in \mathbb{R}^{r \times r}$, $G \in \mathbb{R}^{r \times n_u}$, and $H \in \mathbb{R}^{n_y \times r}$. The form of (9) is equivalent to the following low rank approximations for the full-order state matrices:

$$\begin{bmatrix} A & B \\ C & D \end{bmatrix} \approx \begin{bmatrix} QFQ^T & QG \\ HQ^T & D \end{bmatrix} = \begin{bmatrix} Q & 0 \\ 0 & I_{n_y} \end{bmatrix} \begin{bmatrix} F & G \\ H & D \end{bmatrix} \begin{bmatrix} Q^T & 0 \\ 0 & I_{n_u} \end{bmatrix} \tag{11}$$

The optimal choice for the reduced-order state matrices (F, G, H, D) can be computed given the subspace spanned by Q. This is a similar setup for standard DMD as in in [22–24].

The optimal (reduced-order) state matrices for a given projection space Q are obtained by minimizing the error of the Frobenius norm:

$$\min_{\begin{bmatrix} F & G \\ H & D \end{bmatrix}} \left\| \begin{bmatrix} X_1 \\ Y_1 \end{bmatrix} - \begin{bmatrix} Q & 0 \\ 0 & I \end{bmatrix} \begin{bmatrix} F & G \\ H & D \end{bmatrix} \begin{bmatrix} Q^T & 0 \\ 0 & I \end{bmatrix} \begin{bmatrix} X_0 \\ U_0 \end{bmatrix} \right\|_F^2 \tag{12}$$

As mentioned previously, this is the direct N4SID subspace method for estimating state matrices given measurements of the (reduced-order) state, input, and output. A sub-optimal, but useful, choice for the projection space is given by the POD modes of X_0. The POD modes can be computed by taking the singular value decomposition of $X_0 = U\Sigma V^T$. The POD modes are contained in the columns of U and the relative energy of each mode is contained in the singular values of Σ. These modes provide the spatial component of the flow with the first POD mode being the spatial mode that contains the most energy. The state of the linear system can be approximated on a subspace defined by the first r POD modes of X_0, i.e. $Q := U_r$. The optimal reduced-order state matrices for this choice are given by:

$$\begin{bmatrix} F & G \\ H & D \end{bmatrix}_{opt} = \begin{bmatrix} U_r^T X_1 \\ Y_0 \end{bmatrix} \begin{bmatrix} \Sigma_r V_r^T \\ U_0 \end{bmatrix}^{\dagger} \tag{13}$$

As noted earlier, the primary focus of this paper is developing an algorithm that can achieve the criteria in the beginning of Section 2.1. However, it is important to note that, as with standard DMD, an eigenvalue decomposition of F_{opt} can be used to construct DMD modes. In other words, the eigenvalue decomposition of F_{opt} can be used to construct spatio-temporal modes at a specific temporal frequency for the system. This can be important for control design as was shown in [35]. It should also be noted that this method does not produce a low-dimensional model in balanced coordinates as is done in other model reduction techniques such as balanced truncation, balanced POD, eigensystem realization algorithm, etc. However, this model reduction technique is able to produce a model where the coordinates have some physical meaning and achieve the criteria listed above.

This new methodology also yields input-output information for the model. This proposed method is a tractable implementation of the existing direct N4SID (subspace) method that can be applied to very large systems. This is not simply a black-box (input-output) approach because the state of the reduced-order system z_k can be used to approximately reconstruct the full-order state by:

$$x_k \approx U_r z_k \tag{14}$$

Moreover, the approach requires input/output/state data from the system. Construction and simulation of an adjoint system is not required. The following section will show how to extend this approach to parameter varying systems.

One way to choose the order of the IOROM computed using this approach is to analyze how much energy is captured by the number of modes chosen. It is common to choose the number of modes to capture 99% of the energy (or some similar threshold) in the snapshots. However, for a sufficient model that is suitable for control, the primary metric is the amount of model error incurred from the selection of the number of modes. The model error can be computed using the Frobenius norm:

$$\left\| \begin{bmatrix} X_1 \\ Y_1 \end{bmatrix} - \begin{bmatrix} A & B \\ C & D \end{bmatrix} \begin{bmatrix} X_0 \\ U_0 \end{bmatrix} \right\|_F^2 \tag{15}$$

Again, computation of this model error is intractable for systems with extremely large state dimension. However, the properties of the Frobenius norm can be used to equivalently rewrite this error in a more useful form:

$$\left\| \begin{bmatrix} X_1 \\ Y_1 \end{bmatrix} - \begin{bmatrix} A & B \\ C & D \end{bmatrix} \begin{bmatrix} X_0 \\ U_0 \end{bmatrix} \right\|_F^2 = \left\| \begin{bmatrix} Q^T X_1 \\ Y_1 \end{bmatrix} - \begin{bmatrix} F & G \\ H & D \end{bmatrix} \begin{bmatrix} Q^T X_0 \\ U_0 \end{bmatrix} \right\|_F^2 + \|X_1\|_F^2 - \left\|Q^T X_1\right\|_F^2 \quad (16)$$

The first term represents the model error on the projected subspace. The second and third terms represent the energy lost in the snapshot data X_1 by using the projection. Increasing the number of modes will generally decrease the total error. However, there is a point when adding additional modes will not significantly improve the model error. In fact, adding the modes beyond this point could result in a model that is trying to overfit to the nonlinearities in the system resulting in a degradation of the performance.

2.3. Parameter Varying Approach

This subsection extends the proposed approach in Section 2.2 using a parameter varying linearization similar to the one in [36].

2.3.1. Linearization The parameter varying formulation starts from a nonlinear system that includes an exogenous input, ρ:

$$x_{k+1} = f(x_k, u_k, \rho_k) \quad (17)$$
$$y_k = h(x_k, u_k, \rho_k) \quad (18)$$

The parameter ρ is an exogenous signal that specifies the operating condition. For example, ρ could be a vector of the mean wind speed and direction in the wind farm application or altitude and Mach number for the flexible aircraft example.

Next, assume there is a collection of equilibrium points $(\bar{x}(\rho), \bar{u}(\rho), \bar{y}(\rho))$ such that

$$\begin{aligned} \bar{x}(\rho) &= f(\bar{x}(\rho), \bar{u}(\rho), \rho) \\ \bar{y}(\rho) &= h(\bar{x}(\rho), \bar{u}(\rho), \rho) \end{aligned} \quad (19)$$

If the state is initialized at $x_0 = \bar{x}(\rho)$, the input is held fixed at $u_k = \bar{u}(\rho)$, and the operating condition is frozen at $\rho_k = \rho$ then the state and output will remain in equilibrium at $x_k = \bar{x}(\rho)$ and $y_k = \bar{y}(\rho)$ for $k = 0, 1, \ldots$. Thus $(\bar{x}(\rho), \bar{u}(\rho), \bar{y}(\rho))$ defines an equilibrium condition for each *fixed* value of ρ.

The nonlinear dynamics can be linearized around the equilibrium points defined for each fixed value of ρ. Define perturbations from the equilibrium condition as:

$$\delta x_k := x_k - \bar{x}(\rho), \qquad \delta u_k := u_k - \bar{u}(\rho), \qquad \delta y_k := y_k - \bar{y}(\rho) \quad (20)$$

For a fixed operating condition ($\rho_k = \rho$ for $k = 0, 1, \ldots$), a standard linearization yields:

$$\begin{aligned} \delta x_{k+1} &= A(\rho)\delta x_k + B(\rho)\delta u_k \\ \delta y_k &= C(\rho)\delta x_k + D(\rho)\delta u_k \end{aligned} \quad (21)$$

where the linearized state matrices are defined by

$$\begin{aligned} A(\rho) &:= \left.\frac{\partial f}{\partial x}\right|_{(\bar{x}(\rho), \bar{u}(\rho), \rho)}, \quad B(\rho) := \left.\frac{\partial f}{\partial u}\right|_{(\bar{x}(\rho), \bar{u}(\rho), \rho)} \\ C(\rho) &:= \left.\frac{\partial h}{\partial x}\right|_{(\bar{x}(\rho), \bar{u}(\rho), \rho)}, \quad D(\rho) := \left.\frac{\partial h}{\partial u}\right|_{(\bar{x}(\rho), \bar{u}(\rho), \rho)} \end{aligned} \quad (22)$$

The matrices $(A(\rho), B(\rho), C(\rho), D(\rho))$ define a collection of parameterized LTI systems defined for fixed operating conditions, ρ. Here, we consider the more general case where the operating condition, specified by the parameter ρ_k, varies in time.

Next consider the case where the operating condition, specified by the parameter ρ_k, varies in time. In general $(x_k, u_k, y_k) := (\bar{x}(\rho_k), \bar{u}(\rho_k), \bar{y}(\rho_k))$ is not a valid solution of the nonlinear system. In other words, the parameterized state/input/output values only define an equilibrium condition for fixed values of ρ. Despite this fact, it is still possible to construct a time varying linearization around the parameterized values $(\bar{x}(\rho), \bar{u}(\rho), \bar{y}(\rho))$. Re-define perturbation variables as follows for the case where ρ varies in time:

$$\delta x_k := x_k - \bar{x}(\rho_k), \qquad \delta u_k := u_k - \bar{u}(\rho_k), \qquad \delta y_k := y_k - \bar{y}(\rho_k) \tag{23}$$

A valid (time-varying) linearization can be obtained when ρ_k is time-varying as follows:

$$\delta x_{k+1} = f(x_k, u_k, \rho_k) - \bar{x}(\rho_{k+1}) \tag{24}$$

A Taylor series expansion of $f(x_k, u_k, \rho_k)$ yields:

$$f(\bar{x}_k(\rho_k) + \delta x_k, \bar{u}_k(\rho_k) + \delta u_k, \rho_k) \approx \bar{x}(\rho_k) + A(\rho_k)\delta x_k + B(\rho_k)\delta u_k \tag{25}$$

where A and B are as defined in (22). A similar Taylor series approximation can be performed to linearize the output function h in terms of the matrices C and D defined in (22). Combining (24) and (25) leads to the following parameter varying linearization:

$$\begin{aligned} \delta x_{k+1} &= A(\rho_k)\delta x_k + B(\rho_k)\delta u_k + (\bar{x}(\rho_k) - \bar{x}(\rho_{k+1})) \\ \delta y_k &= C(\rho_k)\delta x_k + D(\rho_k)\delta u_k \end{aligned} \tag{26}$$

This differs from the standard linearization at a single fixed operating point in two respects. First, ρ_k varies in time and hence this is a time-varying system. More precisely, the time variations in the state matrices (A, B, C, D) arise due to ρ_k and hence this is called a linear parameter varying (LPV) system. There are many tools in the controls literature that address this class of systems [37–40]. Second, the equilibrium state varies in time due to the changing operating condition. This effect is retained by the term $\bar{x}(\rho_k) - \bar{x}(\rho_{k+1})$ which provides a forcing term for the dynamics. This model linearizes the dependence on the state and the input. The linearization approximation is accurate as long as the state, input, and output remain near the manifold of equilibrium points $(\bar{x}(\rho_k), \bar{u}(\rho_k), \bar{y}(\rho_k))$. It is important that the nonlinear dependence on the operating condition (specified by ρ_k) is retained.

2.3.2. State Consistency Issue Parameter varying linearizations can be constructed using data from steady operating conditions specified by constant values of ρ. Specifically, the linearization only requires state matrices $(A(\rho), B(\rho), C(\rho),\ D(\rho))$ and equilibrium conditions $(\bar{x}(\rho), \bar{u}(\rho), \bar{y}(\rho))$ at each fixed value of ρ. In principle, the proposed IOROM method or another model reduction method can be used to identify reduced-order state matrices at each operating point, ρ. One key technical issue is state consistency.

To clarify this issue, consider an autonomous system without inputs and outputs. Let $A(\rho)$ denote the state matrix that appears in the parameter varying linearization. DMD can be used at each fixed value of ρ to identify a subspace spanned by $Q(\rho) \in \mathbb{R}^{n_x \times r(\rho)}$ and a reduced-order matrix $F(\rho) \in \mathbb{R}^{r(\rho) \times r(\rho)}$ such that $A(\rho) \approx Q(\rho)F(\rho)Q(\rho)^T$. The reduced-order state at the operating point ρ is defined as $z := Q(\rho)^T \delta x \in \mathbb{R}^{r(\rho)}$. This reduced-order state, z, will lack consistency if the projection subspace $Q(\rho)$ depends on the parameter. In other words, the meaning of z and dimension $r(\rho)$ will depend on the value of ρ. Hence the state, z, at ρ_1 will not, in general, be consistent in either meaning or dimension with the state z at $\rho_2 \neq \rho_1$.

To circumvent this issue, a single consistent subspace $Q \in \mathbb{R}^{n_x \times r}$ should be used at all operating conditions. The reduced-order state $z := Q^T \delta x \in \mathbb{R}^r$ then has a consistent meaning for all parameter values. Moreover, a reduced-order matrix $F(\rho) \in \mathbb{R}^{r \times r}$ can be identified at each value of ρ such that

Algorithm 1 Reduced-Order Parameter Varying Linearization

1: **Given:** Collection of parameter grid points $\{p_g^j\}_{j=1}^{n_g}$.

2: **Data Collection:** At each grid point $j = 1, \ldots, n_g$ do the following:

3: **Equilibrium:** Compute the equilibrium condition $(\bar{x}(p_g^j), \bar{u}(p_g^j), \bar{y}(p_g^j))$ at $\rho = p_g^j$.

4: **Experiment:** Excite the nonlinear system (17) with fixed $\rho_k = p_g^j$. The initial condition x_0 and input u_k should be near the equilibrium condition $(\bar{x}(p_g^j), \bar{u}(p_g^j))$.

5: **Snapshots:** Define the matrices of snapshot deviations from the equilibrium conditions at p_g^j:

$$X_0(p_g^j) := [x_0 - \bar{x}(p_g^j), \ldots, x_{n_s-1} - \bar{x}(p_g^j)] \in \mathbb{R}^{n_x \times n_s} \tag{28}$$

$$X_1(p_g^j) := [x_1 - \bar{x}(p_g^j), \ldots, x_{n_s} - \bar{x}(p_g^j)] \in \mathbb{R}^{n_x \times n_s} \tag{29}$$

$$U_0(p_g^j) := [u_0 - \bar{u}(p_g^j), \ldots, u_{n_s-1} - \bar{u}(p_g^j)] \in \mathbb{R}^{n_u \times n_s} \tag{30}$$

$$Y_0(p_g^j) := [y_0 - \bar{y}(p_g^j), \ldots, y_{n_s-1} - \bar{y}(p_g^j)] \in \mathbb{R}^{n_y \times n_s} \tag{31}$$

6: **Construct Subspace for State Reduction:**

7: **Stack Data:** Define matrix of all state data: $X_0 := [X_0(p_g^1), \ldots, X_0(p_g^{n_g})] \in \mathbb{R}^{n_x \times (n_s n_g)}$.

8: **POD Modes:** Compute POD modes of X_0.

9: **Subspace:** Choose r modes, denoted $Q \in \mathbb{R}^{n_x \times r}$, to capture sufficient energy in X_0.

10: **Reduced-Order State Matrices:** At each grid point $j = 1, \ldots, n_g$ do the following:

11: **IOROM:** Use snapshot data $(X_0(p_g^j), X_1(p_g^j), U_0(p_g^j), Y_0(p_g^j))$ and subspace Q to compute state matrices $(F(p_g^j), G(p_g^j), H(p_g^j), D(p_g^j))$ via the IOROM steps in Section 2.2.

$A(\rho) \approx QF(\rho)Q^T$. This would lead to a reduced-order parameter varying linearization of the form:

$$z_{k+1} = F(\rho_k)z_k + (\bar{z}(\rho_k) - \bar{z}(\rho_{k+1})) \tag{27}$$

where $\bar{z}(\rho) := Q^T\bar{x}(\rho)$ is the equilibrium state projected onto the reduced subspace. The next section presents a method to address this state consistency issue.

2.4. Reduced-Order Parameter Varying Linearizations

One proposed approach for constructing an IOROM for a nonlinear system (1) is shown in Algorithm 1. First, a collection of parameter values are selected (Line 1). Second, data is collected from the nonlinear system at these selected parameter values (Lines 2-5). The collected data includes the equilibrium conditions as well as state/input/output snapshots obtained by exciting the nonlinear system. The algorithm, as written, assumes that the same number of snapshots n_s are obtained at each grid point. However, the number of snapshots can easily change with each grid point. Third, a single r-dimensional subspace of the state space is constructed (Lines 6-9). The subspace, defined by an orthogonal matrix $Q \in \mathbb{R}^{n_x \times r}$, is constructed from the POD modes of the snapshots obtained from *all* parameter values. Fourth, reduced-order state matrices are computed at each parameter vector using the IOROM approach described in Section 2.2 (Lines 10-11).

The outcome of Algorithm 1 is a single r-dimensional subspace Q as well as equilibrium conditions and reduced-order state matrices computed at the selected grid points. This yields a reduced-order parameter varying linearization of the nonlinear system of the form:

$$\begin{aligned} z_{k+1} &= F(\rho_k)z_k + G(\rho_k)\delta u_k + (\bar{z}(\rho_k) - \bar{z}(\rho_{k+1})) \\ \delta y_k &= H(\rho_k)z_k + D(\rho_k)\delta u_k \end{aligned} \tag{32}$$

where $z := Q^T\delta x \in \mathbb{R}^r$ is the reduced-order state and $\bar{z}(\rho) := Q^T\bar{x}(\rho) \in \mathbb{R}^r$ is the reduced-order equilibrium state. The single subspace defined by Q is used to construct state matrices at all

Algorithm 2 Hybrid POD/Gram-Schmidt approach to Construct Subspace

1: **Given:** Collection of parameter grid points $\{p_g^j\}_{j=1}^{n_g}$ and snapshots $X_0(p_g^j)$ from each grid point.
2: **Initial Point:** Use standard POD to compute r_1 modes $Q(p_g^1) \in \mathbb{R}^{n_x \times r_1}$ to capture sufficient energy in $X_0(p_g^1)$.
3: **Iterative Processing:** For $j = 2, \ldots, n_g$, iteratively compute additional modes at each grid point. Given $Q_1 := [Q(p_g^1), \ldots Q(p_g^{j-1})]$, use iterative POD to compute r_j additional modes $Q(p_g^j) \in \mathbb{R}^{n_x \times r_j}$ to capture sufficient energy in $X_0(p_g^j)$.
4: **Subspace:** Stack modes to form a single subspace defined by $Q := [Q(p_g^1), \ldots, Q(p_g^{n_g})]$.

parameter values. Hence the reduced order state z retains a consistent meaning across the parameter domain. Note that Algorithm 1 only computes the state matrices and equilibrium conditions on a grid of specified parameter values. Interpolation (e.g. linear, spline, etc.) must be used to evaluate the state matrices and equilibrium conditions at any parameter value not contained in this grid. It is assumed that the grid of parameter values is sufficiently dense that this interpolation is accurate. The choice of this grid is problem dependent.

The parameter varying linearization can be used to approximate the response of the nonlinear system for an initial condition x_0, input u_k, and parameter trajectory ρ_k. Specifically, the initial condition and input for the nonlinear system define a corresponding initial condition $z_0 = Q^T(x_0 - \bar{x}(\rho_0))$ and input $\delta u_k = u_k - \bar{u}(\rho_k)$ for the parameter varying system. The reduced-order, parameter varying linearization (32) can be simulated to obtain the state response z_k and output δy_k. These correspond to the state response $x_k = Qz_k + \bar{x}(\rho_k)$ and output $y_k = \delta y_k + \bar{y}(\rho_k)$ for the full-order nonlinear system.

The subspace construction step of Algorithm 1 (Lines 6-9) requires the SVD of the matrix X_0 that contains the snapshot data from all the operating points. This matrix has $n_s n_g$ columns and hence the SVD of X_0 may be computationally intractable if there are many grid points. A suboptimal, but more computationally efficient approach, is to iteratively process the snapshot data from each grid point. The basic idea is to determine a set of modes $Q(p_g^1)$ that capture the energy in the snapshots at the first grid point. Next, additional modes $Q(p_g^2)$ are computed so that the combined set $[Q(p_g^1), Q(p_g^2)]$ captures the energy in the snapshots at the second grid point. The procedure continues iteratively computing new modes $Q_2 := Q(p_g^j)$ to combine with previously computed modes $Q_1 := [Q(p_g^1), \ldots, Q(p_g^{j-1})]$. The benefit is that only snapshots obtained from one grid point are required for the calculations. This iterative procedure requires a method to compute the optimal (new) modes Q_2 that should be added to some given modes Q_1. Theorem 1 in the appendix provides a POD-type result to perform this iterative calculation. Algorithm 2 gives the detailed steps for the iterative subspace construction. This method can be thought of as a hybrid POD/Gram-Schmidt approach. Also, it is assumed that the snapshots from one simulation or experiment have comparable amounts of energy, which makes this approach reasonable. This iterative method can replace the single-step method described in Lines 6-9 of Algorithm 1. The remaining steps of Algorithm 1 are unchanged even when combined with the iterative subspace calculation.

There are several benefits of the proposed reduced-order LPV models. The main benefit is that the models can be used for standard, gain-scheduled control. In addition, more formal control analysis and synthesis tools have been developed for LPV systems [37–39]. This LPV modeling approach can yield models that are accurate over a wide range of operating conditions for a nonlinear system. This is in contrast to the existing reduced-order modeling approaches described above which, for the most part, are used to construct a single linear model. In addition, the proposed method relies on input/output data from a forced response and does not require linearization of the system or the construction/simulation of the system adjoint as in BPOD. Finally, the reduced-order model involves a projection onto a well-defined reduced-order subspace. This retains a physical meaning in the reduced-order states. In other words, the reduced-order state can be used to approximate the full-order state of the system. This provides insight into the key spatial modes of fluid/structure systems and is not simply a black-box identification technique, often seen in subspace identification.

The last section in this paper emphasizes the application of this method to develop LPV models for high-dimensional systems.

3. APPLICATION: WIND FARMS

This section demonstrates the proposed IOROM approach on a variation of the low Reynolds number actuator disk example that has been used in wind farm literature [41, 42]. This example has approximately 20,000 states and exhibits highly nonlinear behavior. The IOROM algorithm has also been successfully applied to a more realistic wind farm model using a large eddy simulation with 3.6 million states. Details on that example can be found in [43].

3.0.1. Model Formulation The actuator disk model is considered in this paper as a demonstration of the proposed parameter varying IOROM approach [41,42]. The actuator disk is used to represent wind turbines in the flow field. In this specific example, we will use two turbines, one directly downstream of the other, see Figure 1. The flow within the two turbine array is modeled using the two-dimensional unsteady, incompressible, Navier-Stokes equations. The typical operating wind speeds in a wind farm do not exceed 25 m/s. This is low relative to the speed of sound at sea level ($\sim$300 m/s) and hence it is sufficient to assume incompressibility [44]. Let (u, v) [m/s] denote the streamwise and spanwise velocity components and (x, y) [m] denote the streamwise and spanwise distance. Under these assumptions, the nondimensionalized dynamics for (u, v) are governed by the following partial differential equations:

$$\frac{\partial \mathrm{u}}{\partial \mathrm{x}} + \frac{\partial \mathrm{v}}{\partial \mathrm{y}} = 0 \tag{33}$$

$$\frac{\partial \mathrm{u}}{\partial t} + \mathrm{u}\frac{\partial \mathrm{u}}{\partial \mathrm{x}} + \mathrm{v}\frac{\partial \mathrm{u}}{\partial \mathrm{y}} = -\frac{\partial \mathrm{p}}{\partial \mathrm{x}} + \frac{1}{Re}\left(\frac{\partial^2 \mathrm{u}}{\partial \mathrm{x}^2} + \frac{\partial^2 \mathrm{u}}{\partial \mathrm{y}^2}\right) + f_{\mathrm{x},1} + f_{\mathrm{x},2} \tag{34}$$

$$\frac{\partial \mathrm{v}}{\partial t} + \mathrm{u}\frac{\partial \mathrm{v}}{\partial \mathrm{x}} + \mathrm{v}\frac{\partial \mathrm{v}}{\partial \mathrm{y}} = -\frac{\partial \mathrm{p}}{\partial \mathrm{y}} + \frac{1}{Re}\left(\frac{\partial^2 \mathrm{v}}{\partial \mathrm{x}^2} + \frac{\partial^2 \mathrm{v}}{\partial \mathrm{y}^2}\right) + f_{\mathrm{y},1} + f_{\mathrm{y},2} \tag{35}$$

where p is pressure in the flow, Re is the Reynolds number, and f_{x} is a force turbines apply to the flow in the x direction. The equations have been nondimensionalized by Re. Re is defined as the ratio of inertial forces to viscous forces: $\frac{U_\infty \mathrm{D}}{\nu}$ where U_∞ is the freestream velocity [m/s], D is the diameter of the turbine [m], and ν is the kinematic viscosity [m^2/s]. By changing Re in this example, it is effectively changing the freestream velocity. The dynamics of the system vary depending on the parameter, Re, that is being simulated.

The loading of each turbine is defined linearly. Specifically, assume that all spatial units have been nondimensionalized by the turbine diameter D. If the hub of the upstream turbine is placed at $\mathrm{x} = \mathrm{x}_1$ and $\mathrm{y} = \mathrm{y}_1$ then the rotor plane lies within $\mathrm{y}_1 - \frac{1}{2} \leq \mathrm{y} \leq \mathrm{y}_1 + \frac{1}{2}$. The forcing term introduced by the turbines is then given by:

$$f_{\mathrm{x},i}(\mathrm{x}, \mathrm{y}, t) := \begin{cases} k_{T_\mathrm{x},i} C_{T,i}(a_i(t))(\mathrm{y} - \mathrm{y}_i) & \text{if } \mathrm{x} = \mathrm{x}_i \ \& \ |\mathrm{y} - \mathrm{y}_i| \leq 0.5 \\ 0 & \text{else} \end{cases} \tag{36}$$

$$f_{\mathrm{y},i}(\mathrm{x}, \mathrm{y}, t) := \begin{cases} k_{T_\mathrm{y},i} C_{T,i}(a_i(t))(1 - |\mathrm{x} - \mathrm{x}_i|) & \text{if } \mathrm{y} = \mathrm{y}_i \ \& \ |\mathrm{x} - \mathrm{x}_i| \leq 0.1 \\ 0 & \text{else} \end{cases} \tag{37}$$

where $i = 1, 2$ indicates the upstream and downstream turbines. Note that f_x is defined such that it will introduce an asymmetry to the flow that will induce wake meandering. The constant $k_T := U_{in,i}$, U_{in} is the average nondimensionalized velocity across the rotor, and $C_{T,i}$ is the thrust coefficient of the turbine, which is a function of the turbine operation, i.e. the axial induction

factor, a. According to actuator disk theory, C_T can be related to the axial induction factor by: $C_T = 4a(1-a)$ [45]. Physically, the axial induction factor is a measure of how much the wind slows down due to the action of the turbine. The optimal operating point is $a = \frac{1}{3}$. In this particular example, a_2 is the single input to this system, i.e. a_1 is fixed at the optimal operating point and a_2 is allowed to vary about the optimal operating point. The loading magnitude can be changed by the thrust coefficient. On utility-scale turbines, this would be equivalent to changing the blade pitch angle or generator torque [1, 45]. These equations are solved using standard CFD methods [46]. Specifically, a central differencing scheme was used for the two-dimensional actuator disk model. The grid is defined by N_{x} points in the streamwise x direction and N_{y} point in the spanwise y direction. For this actuator disk model, the typical spacing between grid points is $\delta\text{x} = 0.1$ and $\delta\text{y} = 0.1$ with a typical time step of $\delta t = 0.01$.

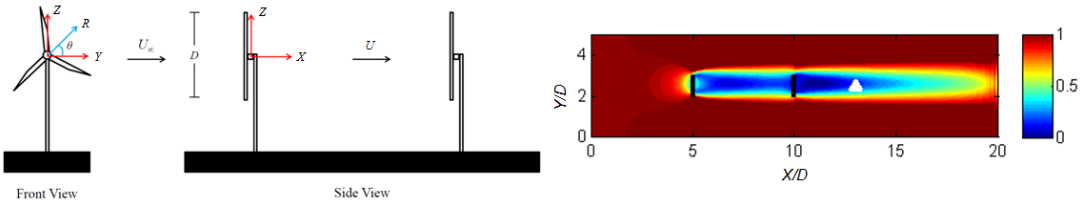

Figure 1. Two-turbine setup (left) and the corresponding baseflow (right) for the low Re flow specified. It should be noted that the flow is depicted as if you are looking at the two-turbine array from above.

The setup has two turbines spaced 5D apart in the streamwise direction. There is a point 3D downstream of the second turbine where the wind speed is measured (indicated by the white triangle in Figure 1). For simplicity, as mentioned above, we assume that we can only control the wind speed by actuating the second turbine. As a result, the system that will be identified will be a single-input-single-output system where the input is the axial induction factor of the downstream turbine, a_2, and the output is the spanwise velocity, v at the white triangle in Figure 1. In addition, the domain in the streamwise direction was set to 20D with 201 grid points and in the spanwise direction was set to 5D with 51 grid points. This would amount to 20,000 states for this particular example by having 2 velocity components per grid point. More realistic, higher fidelity codes for wind farms will have even larger state dimensions [2,47]. It is important to note that the Re used in these simulations will be on the order of 10. This is a low Re in comparison with the Re typically experienced by wind farms, which is on the order of 10^6.

3.0.2. IOROM Method: Single Operating Point First, the IOROM method discussed in Section 2.2 will be implemented for the actuator disk problem at one particular operating point, i.e. a single Re. We will use Algorithm 1, but as examples become larger than this, i.e. large eddy simulations where the states are on the order of millions rather than tens of thousands, Algorithm 2 will have to be implemented. One way to do is to use the technique used for large streaming data sets in [48].

The IOROM method is used to construct a single time-invariant model with Re held constant. The system is simulated with $Re = 50$ and $a_2 = u = 1/3$, i.e. the downstream turbine input is fixed at the optimal operating point, to determine the equilibrium point $\bar{x}(Re)$ for this parameter value. Next, the nonlinear system (33) is excited for $T_f = 100$ s (recall the timestep for this simulation is 0.01 s). This system is excited at the second turbine with a chirp excitation input $u(t) = 0.250.25\sin(\omega(t)t)$, where $\omega(t) = 0.0628(50)^{\frac{t}{T_f}}$ [rad/s]. This excites the nonlinear system with frequencies from 0.01 to 0.2 Hz. The nonlinear system is simulated and snapshots of the state/input/output are collected every 0.5 s. This yields 200 snapshots over the 100 s simulation.

Using the IOROM approach, we were able to construct a model with 20 states. This was selected by examining the model fitting error. Because the state dimension is large, the model fitting error cannot be computed directly. Instead, (16) was used to compute the model fitting error. The model error decreases as more modes are used but begins to plateau at 20 modes, see Figure 2. At this point, there is minimal benefits to increasing the order of the model. As stated previously, it is possible

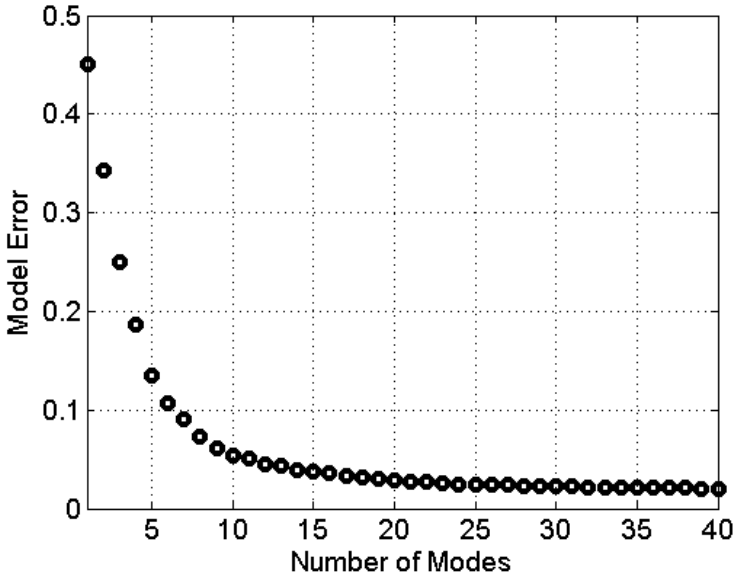

Figure 2. Model fitting error computed for the actuator disk example using the IOROM technique.

that the performance of the model will degrade as the model order increases because the model will be overfitting to the nonlinearities of the system.

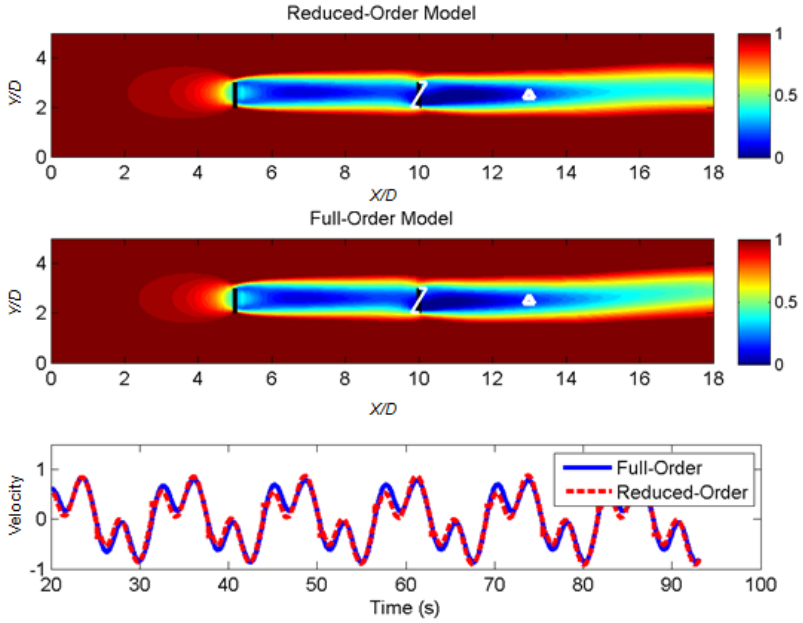

Figure 3. IOROM Results of the actuator disk example. The top plot shows the flow field reconstructed using 20 modes. The middle plot shows the full-order nonlinear flow. The bottom plot shows the output (indicated by the triangle in the top and middle plot) of the reduced-order model compared to the full-order model. The output for this particular example is the velocity fluctuations at the measurement point $3D$ downstream of the second turbine.

The reduced-order model was validated using a square wave as an input to the second turbine. The results can be seen in Figure 3. One of the main advantages to this method is that the full

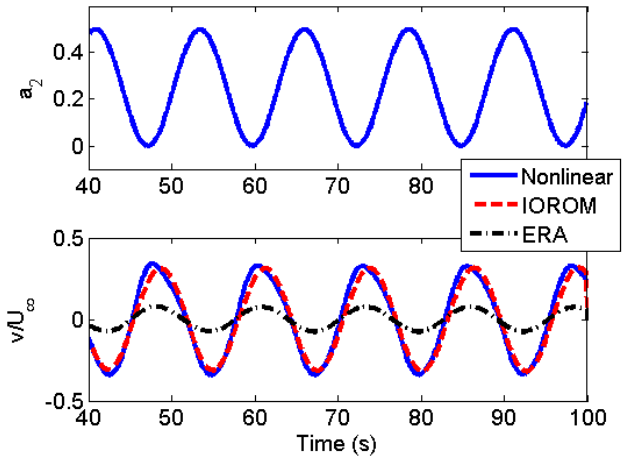

Figure 4. This plot shows the output of the reduced-order models constructed using ERA and the IOROM approach proposed in this paper. The output for this particular example is the velocity fluctuations at the measurement point $3D$ downstream of the second turbine.

state can be reconstructed from the reduced-order state. Figure 3 shows the results of the reduced-order model as compared to the full-order model. The top plot shows the reconstructed flow field from the 20 state model identified from the IOROM approach. The middle plot shows the full-order actuator disk model. Visually, the top plot and the middle plot show good agreement. The bottom plot shows the output; i.e. the velocity measured 3D downstream of the second turbine. The output of the reduced-order model closely matches the output of the full-order model.

The IOROM technique that was used to identify a low-order model for the actuator disk example was compared to another existing technique, eigensystem realization algorithm (ERA), that is capable of constructing an input/output model. It is important to note that the model generated by ERA is in balanced coordinates, which can be useful in identifying the most observable and controllable states of the system. However, this is also a drawback in the sense that these coordinates do not have physical meaning and are difficult to incorporate into a scheduling/parameter varying model. This IOROM technique has also been compared to BPOD in [49]. A separate simulation was run to obtain the impulse response data necessary for ERA using an impulse as an input. The model obtained from the IOROM approach and ERA are both obtained for a single operating point, i.e. $Re = 50$.

Figure 4 shows the results of the input/output relationship obtained using ERA and the IOROM approach on the actuator disk example. In Figure 4, the input to the system is shown on the top, where $u(t) = 0.25 + 0.25\sin(0.5t)$. The output of the reduced-order models are shown on the bottom plot. This bottom plot shows that ERA has a difficult time identifying the system at this particular operating point. This is in part due to the excitation signal. With the IOROM technique, a chirp signal was used, which excites the dynamics at a range of frequencies. With ERA, an impulse is used and is unable to capture the essential dynamics of the system. This IOROM technique has a much larger excitation energy than the impulse used by ERA. This allows the IOROM to capture a better input/output model. However, to use this IOROM approach, the system must be of the form where it is easily excitable by a controllable input. It should be noted that ERA has been extended to include non-impulse inputs using observer Kalman identification (OKID) [15]. This ERA-OKID approach was applied to the actuator disk problem and no performance benefit was observed in comparison with ERA. This is likely due to the strong nonlinearities present in this particular example. This indicates that the additional state information used with the input/output data for the IOROM approach can help identify a low-dimensional model for the actuator disk example. Lastly, it should be noted that ERA has been extended to a time-varying framework in [12–14]. A

comparison between this IOROM approach and other time varying approaches will be explored in future work.

3.0.3. IOROM Parameter Varying Method The parameter varying method described in Section 2.4 is used to construct parameter varying reduced-order models. A grid of five parameter values was selected, $Re_j = \{10 : 10 : 50\}$. At each fixed value of Re in this grid, the system was simulated with $u = 0$ to determine the corresponding equilibrium point, $\bar{x}(Re_j)$. Next, the nonlinear system is excited for $T_f = 100$ s at each Re_j with a chirp excitation input $u(t) = 0.25 + 0.25\sin(\omega(t)t)$, where $\omega(t) = 0.0628(50)^{\frac{t}{T_f}}$. The Re changes the effective wind speed of the simulation which changes the dynamics within the system. For example, wake meandering is an oscillation that happens in this particular flow due to the instabilities in the wake. Wake meandering instabilities increase, i.e. the magnitude increases, as the Re increases in this particular example. The chirp signal frequencies were chosen to capture the wake meandering frequency. The chirp signal excites the nonlinear system at frequencies between 0.01 Hz to 0.5 Hz. Again, the nonlinear system is simulated and snapshots of the state/input/output are collected every 0.5 s. This yields 200 snapshots over the $T_f = 100$ s simulation for each parameter grid point.

The basic single step procedure (Algorithm 1) is used to construct the subspace modes Q. This example is small enough that it was possible to compute the SVD on snapshots obtained at all grid points. In addition, a MapReduce technique in [50] can be used to compute the SVD of large, tall-skinny matrices. Twenty modes were selected and reduced-order models were constructed at each grid point using the IOROM procedure.

Lastly, Figure 5 compares a time-domain step response of the full-order nonlinear system and the reduced-order LPV model. The Re varies at $Re(t) = 25 - 10\sin(0.1t)$. The controllable input was a square wave where the amplitude was 0.25 with a 50% duty cycle. The nonlinear system was simulated with a time step of 0.01 s and the reduced-order parameter varying model was simulated with a time step of 0.5 s. Linear interpolation was used to compute the state matrices and equilibrium points appearing in the LPV model for parameter values not contained in the five point grid. It should be emphasized that a different input signal was used for the validation of this LPV model and the simulation is varying across a wide range of Re. The input/output relationship of the reduced-order LPV model is in close agreement with the full-order nonlinear system. These results indicate that this reduced-order LPV model can be used for predictive purposes and/or control design.

4. CONCLUSION

This paper described a method to construct reduced-order models for high-dimensional nonlinear systems. It is assumed that the nonlinear system has a collection of equilibrium operating points. The method has two main components. First, a reduced-order linear system is constructed at each equilibrium point using input/output data. Second, a parameter varying linearization is used to connect these linear models. A nonlinear actuator disk example was used to demonstrate this method. Future work will apply this method to construct reduced-order parameter varying models for wind farm control using higher-fidelity models.

5. ACKNOWLEDGMENTS

This work was partially supported by the National Science Foundation under Grant No. NSF-CMMI-1254129 entitled “CAREER: Probabilistic Tools for High Reliability Monitoring and Control of Wind Farms”. The work was also supported by the University of Minnesota Institute on the Environment, IREE Grant No. RS-0039-09.

The first author gratefully acknowledges the financial support from the University of Minnesota through the 2015-16 Doctoral Dissertation Fellowship. The authors would also like to thank Joseph Nichols for discussions on this topic as well as help implementing the actuator disk example.

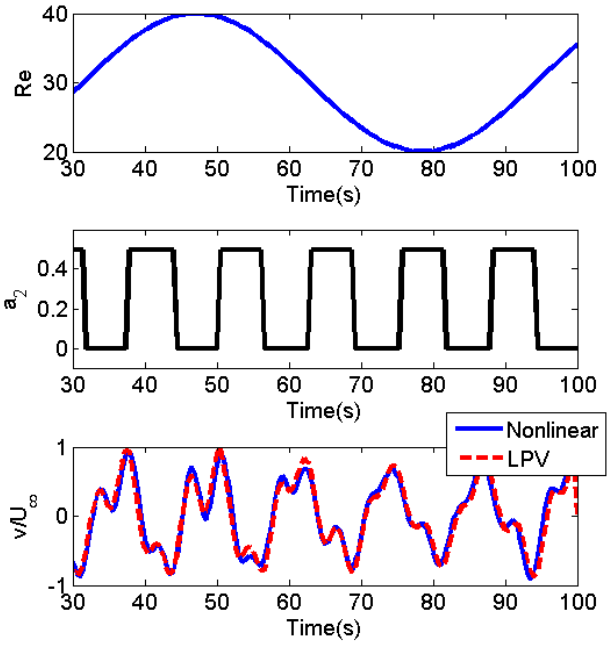

Figure 5. Time domain signal of the Reynolds number, input, and output. The output of the reduced-order LPV model is compared to the full-order nonlinear simulation. Note that the input is the turbine forcing on the downstream turbine and the output is the velocity fluctuations $3D$ downstream of the second turbine.

REFERENCES

1. Johnson KE, Thomas N. Wind farm control: addressing the aerodynamic interaction among wind turbines. *American Control Conference (ACC)*, IEEE, 2009; 2104–2109.
2. Churchfield M, Lee S. NWTC design codes-SOWFA 2012; .
3. Yang X, Sotiropoulos F, Conzemius RJ, Wachtler JN, Strong MB. Large-eddy simulation of turbulent flow past wind turbines/farms: the virtual wind simulator (VWiS). *Wind Energy* 2015; **18**(12):2025–2045.
4. Beranek J, Nicolai L, Buonanno M, Burnett E, Atkinson C, Holm-Hansen B, Flick P. Conceptual design of a multi-utility aeroelastic demonstrator. *13th AIAA/ISSMO Multidisciplinary Analysis Optimization Conference*, 2010; AIAA–2010–9350.
5. Lind R, Brenner M. *Robust aeroservoelastic stability analysis*. Springer-Verlag, 1999.
6. MSC Software Corporation. *MSC/NASTRAN: Structural and Multidiscipline Finite Element Analysis* 2012.
7. Danowsky B, Thompson P, Farhat C, Lieu T, Harris C, Lechniak J. Incorporation of feedback control into a high-fidelity aeroservoelastic fighter aircraft model. *Journal of Aircraft* 2010; **47**(4):1274–1282.
8. Zhou K, Doyle JC, Glover K. *Robust and optimal control*. Prentice hall New Jersey, 1996.
9. Viberg M. Subspace-based methods for identification of linear time-invariant systems. *Automatica* 1995; **31**(12):1835–1851.
10. Lall S, Marsden J, Glavaški S. A subspace approach to balanced truncation for model reduction of nonlinear control systems. *International journal of robust and nonlinear control* 2002; **12**(6):519–535.
11. Juang JN, Pappa RS. An eigensystem realization algorithm for modal parameter identification and model reduction. *Journal of guidance, control, and dynamics* 1985; **8**(5):620–627.
12. Majji M, Juang JN, Junkins JL. Observer/kalman-filter time-varying system identification. *Journal of guidance, control, and dynamics* 2010; **33**(3):887–900.
13. Majji M, Juang JN, Junkins JL. Time-varying eigensystem realization algorithm. *Journal of guidance, control, and dynamics* 2010; **33**(1):13–28.
14. Majji M, Juang JN, Junkins JL. Time-varying deadbeat controller design. *Journal of Guidance, Control, and Dynamics* 2012; **35**(1):284–295.
15. Juang JN, Phan M, Horta LG, Longman RW. Identification of observer/kalman filter markov parameters-theory and experiments. *Journal of Guidance, Control, and Dynamics* 1993; **16**(2):320–329.
16. Loéve M. *Probability Theory*. Van Nostrand, 1955.
17. Berkooz G, Holmes P, Lumley J. The proper orthogonal decomposition in the analysis of turbulent flows. *Annual Review of Fluid Mechanics* 1993; **25**:539–575.
18. Holmes P, Lumley J, Berkooz G. *Turbulence, Coherent Structures, Dynamical Systems and Symmetry*. Cambridge University Press, 1988.

19. Willcox K, Peraire J. Balanced model reduction via the proper orthogonal decomposition. *AIAA journal* 2002; **40**(11):2323–2330.
20. Rowley C. Model reduction for fluids using balanced proper orthogonal decomposition. *International Journal of Bifurcation and Chaos* 2005; **15**(03):997–1013.
21. Ma Z, Ahuja S, Rowley CW. Reduced-order models for control of fluids using the eigensystem realization algorithm. *Theoretical and Computational Fluid Dynamics* 2011; **25**(1-4):233–247.
22. Schmid P. Dynamic mode decomposition of numerical and experimental data. *Journal of Fluid Mechanics* 2010; **656**:5–28.
23. Schmid P, Li L, Juniper M, Pust O. Applications of the dynamic mode decomposition. *Theoretical and Computational Fluid Dynamics* 2010; **25**:249–259.
24. Tu JH, Rowley CW, Luchtenburg DM, Brunton SL, Kutz JN. On dynamic mode decomposition: Theory and applications. *Journal of Computational Dynamics* 2014; **1**(2):391–421.
25. Budišić M, Mohr R, Mezić I. Applied koopmanisma). *Chaos: An Interdisciplinary Journal of Nonlinear Science* 2012; **22**(4):047 510.
26. Mezic I. Analysis of fluid flows via spectral properties of the Koopman operator. *Annual Review of Fluid Mechanics* 2013; **45**:357–378.
27. Rowley CW, Mezić I, Bagheri S, Schlatter P, Henningson DS. Spectral analysis of nonlinear flows. *Journal of fluid mechanics* 2009; **641**:115–127.
28. Proctor J, Brunton S, Kutz J. Dynamic mode decomposition with control. *SIAM Journal on Applied Dynamical Systems* 2016; **15**:142–161.
29. Danowsky B, Lieu T, Coderre-Chabot A. Control oriented aeroservoelastic modeling of a small flexible aircraft using computational fluid dynamics and computational structural dynamics. *Proceedings of the AIAA SciTech Conference, San Diego, CA*, 2016.
30. Poussot-Vassal C, Roos C. Generation of a reduced-order LPV/LFT model from a set of large-scale mimo lti flexible aircraft models. *Control Engineering Practice* 2012; **20**(9):919–930.
31. Hemati MS, Dawson ST, Rowley CW. Unsteady aerodynamic response modeling: A parameter-varying approach. *53rd AIAA Aerospace Sciences Meeting*, 2015; 1069.
32. Gugercin S, Antoulas AC, Beattie C. H_2 model reduction for large-scale linear dynamical systems. *SIAM journal on matrix analysis and applications* 2008; **30**(2):609–638.
33. Poussot-Vassal C, Sipp D. Parametric reduced order dynamical model construction of a fluid flow control problem. *IFAC-PapersOnLine* 2015; **48**(26):133–138.
34. Panzer H, Mohring J, Eid R, Lohmann B. Parametric model order reduction by matrix interpolation. *at-Automatisierungstechnik Methoden und Anwendungen der Steuerungs, Regelungs-und Informationstechnik* 2010; **58**(8):475–484.
35. Mengali G. Role of eigenvectors in aircraft dynamics optimization. *Journal of guidance, control, and dynamics* 2003; **26**(2):340–346.
36. Takarics B, Seiler P. Gain scheduling for nonlinear systems via integral quadratic constraints. *American Control Conference (ACC)*, IEEE, 2015; 811–816.
37. Packard A. Gain scheduling via linear fractional transformations. *Systems and Control Letters* 1994; **22**:79–92.
38. Wu F. A generalized LPV system analysis and control synthesis framework. *International Journal of Control* 2001; **74**:745–759.
39. Scherer C. *Advances in linear matrix inequality methods in control*, chap. Robust mixed control and linear parameter-varying control with full-block scalings. SIAM, 2000; 187–207.
40. Pfifer H, Seiler P. Robustness analysis of linear parameter varying systems using integral quadratic constraints. *International Journal of Robust and Nonlinear Control* 2014; doi:10.1002/rnc.3240.
41. Sørensen JN, Myken A. Unsteady actuator disc model for horizontal axis wind turbines. *Journal of Wind Engineering and Industrial Aerodynamics* 1992; **39**(1):139–149.
42. Sørensen JN, Kock CW. A model for unsteady rotor aerodynamics. *Journal of wind engineering and industrial aerodynamics* 1995; **58**(3):259–275.
43. Annoni J, Gebraad P, Seiler P. Wind farm flow modeling using input-output dynamic mode decomposition. *accepted to the American Control Conference (ACC)*, 2016.
44. Schlichting H, Gersten K. *Boundary-layer theory*. Springer Science & Business Media, 2003.
45. Burton T, Sharpe D, Jenkins N, Bossanyi E. *Wind energy handbook*. John Wiley & Sons, 2001.
46. Zikanov O. *Essential computational fluid dynamics*. John Wiley & Sons, 2010.
47. Yang X, Sotiropoulos F, Conzemius R, Wachtler J, Strong M. Large-eddy simulation of turbulent flow past wind turbines/farms: the virtual wind simulator (VWiS). *Wind Energy* 2014; .
48. Hemati MS, Williams MO, Rowley CW. Dynamic mode decomposition for large and streaming datasets. *Physics of Fluids (1994-present)* 2014; **26**(11):111 701.
49. Annoni J, Nichols J, Seiler P. Wind farm modeling and control using dynamic mode decomposition. *34th Wind Energy Symposium*, 2016; 2201.
50. Dean J, Ghemawat S. Mapreduce: simplified data processing on large clusters. *Communications of the ACM* 2008; **51**(1):107–113.

Theorem 1
Let $Q_1 \in \mathbb{R}^{n_x \times r_1}$ be a given matrix with $Q_1^T Q_1 = I_{r_1}$. Let $X \in \mathbb{R}^{n_x \times n_s}$ be given snapshot data.

Define the SVD of the projected snapshot matrix $(I_{n_x} - Q_1 Q_1^T)X = U\Sigma V^T$. Let r_2 be any non-negative integer such that $r_2 \leq rank((I_{n_x} - Q_1 Q_1^T)X)$ and $\sigma_{r_2} > \sigma_{r_2+1}$. Then

$$\min_{\substack{Q_2 \in \mathbb{R}^{n_x \times r_2},\, Q_2^T Q_2 = I_{r_2} \\ C_1 \in \mathbb{R}^{r_1 \times n_s} \\ C_2 \in \mathbb{R}^{r_2 \times n_s}}} \|X - Q_1 C_1 - Q_2 C_2\|_F^2 = \sum_{k=r_2+1}^{rank(X)} \sigma_k^2 \tag{38}$$

An optimal solution is given by $C_{1,opt} = Q_1^T X$, $Q_{2,opt} = U_r$, and $C_{2,opt} = \Sigma_r V_r^T$ where Σ_r, U_r, and V_r are associated with the first r singular values and vectors of $(I_{n_x} - Q_1 Q_1^T)X$.

Proof
Use Gram-Schmidt orthogonalization to construct a matrix $Q_{1,\perp} \in \mathbb{R}^{n_x \times (n_x - r_1)}$ such that $\begin{bmatrix} Q_1 & Q_{1,\perp} \end{bmatrix}$ is orthogonal. The orthogonal invariance of the Frobenius norm thus implies

$$\|X - Q_1 C_1 - Q_2 C_2\|_F^2 = \left\| \begin{bmatrix} Q_1^T \\ Q_{1,\perp}^T \end{bmatrix} (X - Q_1 C_1 - Q_2 C_2) \right\|_F^2 = \left\| \begin{bmatrix} Q_1^T X - C_1 - Q_1^T Q_2 C_2 \\ Q_{1,\perp}^T X - Q_{1,\perp}^T Q_2 C_2 \end{bmatrix} \right\|_F^2 \tag{39}$$

The second equality follows from $Q_1^T Q_1 = I_{r_1}$ and $Q_{1,\perp}^T Q_1 = 0_{(n_x - r_1) \times r_1}$. The error can be split as:

$$\|X - Q_1 C_1 - Q_2 C_2\|_F^2 = \|Q_1^T X - C_1 - Q_1^T Q_2 C_2\|_F^2 + \|Q_{1,\perp}^T X - Q_{1,\perp}^T Q_2 C_2\|_F^2 \tag{40}$$

The second term is unaffected by the choice of C_1. Moreover, for any (Q_2, C_2) the first term can be made equal to zero by the choice $C_{1,opt} = Q_1^T X - Q_1^T Q_2 C_2$. In fact, $Q_1^T Q_2 = 0$ may be assumed without loss of generality. Specifically, the choice of Q_2 only affects the second term of (40) (assuming the optimal choice for C_1 just specified). Perform a change of variables $Q_2 = \begin{bmatrix} Q_1 & Q_{1,\perp} \end{bmatrix} \begin{bmatrix} \tilde{Q}_2 \\ \hat{Q}_2 \end{bmatrix}$. This change of variables from Q_2 to $\begin{bmatrix} \tilde{Q}_2 \\ \hat{Q}_2 \end{bmatrix}$ is invertible since $\begin{bmatrix} Q_1 & Q_{1,\perp} \end{bmatrix}$ is orthogonal. Substitute this change of variables into the second error term to obtain $\|Q_{1,\perp}^T X - Q_{1,\perp}^T Q_2 C_2\|_F^2 = \|Q_{1,\perp}^T X - \hat{Q}_2 C_2\|_F^2$. Thus $\tilde{Q}_2$ has no effect on the second term and may be set to zero. Q_2 can be selected to have the form $Q_{1,\perp}\hat{Q}_2$ and hence $Q_1^T Q_2 = 0$. In this case, the optimal choice for C_1 simplifies to $C_{1,opt} = Q_1^T X$.

Retaining the assumption that $Q_1^T Q_2 = 0$ as well as $C_{1,opt} = Q_1^T X$, the total error is given by:

$$\|X - Q_1 C_1 - Q_2 C_2\|_F^2 = \|(I_{n_x} - Q_1 Q_1^T)X - Q_2 C_2\|_F^2 \tag{41}$$

By the standard POD result this cost is minimized by the choice $Q_{2,opt} = U_r$, and $C_{2,opt} = \Sigma_r V_r^T$ where Σ_r, U_r, and V_r are associated with the first r singular values and vectors of $(I_{n_x} - Q_1 Q_1^T)X$. It can be shown that this construction satisfies the assumption $Q_1^T Q_{2,opt} = 0$. □